Further Data On Sesamoid Identity From Two Anuran Species

MIRIAM CORINA VERA,[1] MARÍA LAURA PONSSA,[1]* AND VIRGINIA ABDALA[2]
[1]Unidad Ejecutora Lillo, Instituto de Herpetología, CONICET-Fundación Miguel Lillo, Miguel Lillo 251, San Miguel de Tucumán 4000, Argentina
[2]Instituto de Biodiversidad Neotropical, UNT—CONICET, Cátedra de Biología General, Facultad de Ciencias Naturales e IML, UNT. Miguel Lillo 205, San Miguel de Tucumán 4000, Argentina

ABSTRACT

Considering that the identification of equivalent entities is the basis for any comparative analysis, we compare the histology, histochemistry, shape and dimensions of epiphyses, carpal and sesamoids in two anuran frogs. Our goal was to explore the morphological correspondence among these three skeletal elements in order to clarify the sesamoid identity. We studied the skeletogenesis, contour geometric morphometry and dimensions of forelimb elements of juveniles of two anurans species *Leptodactylus bufonius* and *Rhinella arenarum*. Skeletogenesis in anurans present a common trait between carpals and sesamoids: both elements exhibit endochondral ossification. A difference between these elements is the presence of fibrocartilage in the development of sesamoids. The geometric morphometry does not allow us to establish a shape pattern that can be compared either between sesamoids and epiphyses or carpals. With regard to dimensions, our data indicate that bones categorization based on these aspects is ambiguous and therefore is useless to classify of skeletal bones. The data about tissue differentiation of sesamoids provide evidence that support the idea that these elements should be considered part of the typical endowment of the vertebrate skeleton. Anat Rec, 00:000–000, 2015.

Key words: histochemistry; histology; morphometry; forelimb; frog; juveniles

The forelimb skeleton of tetrapods is composed of three elements: long bones, short bones (carpals) and sesamoids. Short bones are those having their three dimensions equally developed, with a thin cortex of compact bone tissue and spongy bone tissue inside (Tortora and Derrickson, 2006; Ross and Pawlina, 2007). The word sesamoid comes from seed-like, morphology as sesame seed (Vickaryous and Olson, 2007). These elements are rarely mentioned in the descriptions of normal anatomy of any tetrapod skeleton because of their alleged variability (but see Jerez et al., 2009; Ponssa et al., 2010). It has been proposed that sesamoids originate through persistent mechanical stimuli on tendons that wrap around an epiphysis (Carter et al., 1998). However, Ponssa et al. (2010) demonstrate that differentiation of many sesamoids begins well before the tendinous tissue is recognizable. Their histological data show that the main stimulus eliciting the graciella sesamoid genesis

Abbreviations used: ECM = extracellular matrix; PCA = principal component analysis

Grant sponsor: ANPCyT; Grant number: BID-PICT 616, PICT 2011-1524, PICT 2013-0404; Grant sponsor: CONICET; Grant numbers: PIP 0284. FONCyT, PICT 2011-1524; PICT 2010-0616. UNT, G519.

*Correspondence to: María Laura Ponssa, Unidad Ejecutora Lillo, Instituto De Herpetología, CONICET-Fundación Miguel Lillo, Miguel Lillo 251, San Miguel De Tucumán 4000, Argentina. E-mail: mlponssa@hotmail.com

Received 10 November 2014; Accepted 26 January 2015.

DOI 10.1002/ar.23158
Published online 00 Month 2015 in Wiley Online Library (wileyonlinelibrary.com).

should be genetic because the cartilage precursor is present before the dense connective tissue differentiates into a tendon (Ponssa et al., 2010). They also interpreted that if a whole group includes a particular sesamoid, it will be constant, and its origin could be mainly linked to genetic stimulus; lack of regularity could be showing a preeminence of extrinsic factors over those genetic ones (Ponssa et al., 2010). Thus, sesamoid origin is still a matter of debate (Le Minor, 1987; Giori et al., 1993; Carter et al., 1998; Sarin et al., 1999; Ponssa et al., 2010).

The development of the sesamoids in tetrapods was studied generally in larval/postnatal and adult stages (Bland and Ashhurst, 1997; Doherty, 2010; Olson, 2000; Prochel, 2006; Kim et al., 2009; Ponssa et al., 2010; Shearman and Maglia, 2015). In lizards, many sesamoids appear in post-hatching specimens (Jerez et al., 2009). Fabrezi et al. (2007) showed that sesamoids of this group undergo endochondral ossification, a complex process by which the growth cartilage within the bone cortex is progressively replaced by bone tissue (Felisbino and Carvalho, 2001). Doherty (2010) provided data of endochondral ossification of sesamoids in mammals. She described the presence of hypertrophic chondrocytes within the calcifying core of the sesamoid, similar to that observed in the epiphyseal growth plates of the phalanges and metapodophalangeal bones. In anurans, data about sesamoid skeletogenesis are very scarse (Ponssa et al., 2010), they appear mostly at metamorphic stages, reaching a cartilaginous phase at the moment of the metamorphosis (Ponssa et al., 2010; Vera and Ponssa, 2014).

The juvenile period in anurans typically involves the passage from aquatic to terrestrial environments (McDiarmid and Altig, 1999; Fabrezi et al., 2014); thus, it is a critical phase in the development of the osteological elements, because they affect the locomotor capacity of the froglet and its adaptation to the terrestrial habitat (Vera and Ponssa, 2014). The changes in the skeletal tissue development occurring through the juvenile phase - when the limbs are fully functional- are relevant to understand its relation with the acquisition of locomotor capacities. In spite of the pervasive relationship that has been proposed between sesamoids and locomotion (Sarin et al., 1999; Vickaryous and Olson, 2007), data about skeletogenesis of these structures during the juvenile anuran stages are lacking. In this work we present data about the skeletogenesis of the sesamoids in juveniles of two anuran species, and relate them with the acquisition of terrestrial locomotion.

Bone classifications based on their shape have been widely used (Tortora and Derrickson, 2006; Ross and Pawlina, 2007) highlighting the biological meaning attributed to shape. Thus, it can be a source of evidence to find out whether sesamoids could be defined as short bones. Methodologies such as morphometric geometry allow a rigorous analysis of shape variations.

Here, we integrate several lines of evidence as an attempt of to fill the gaps in our knowledge of sesamoids, probably one of the most neglected and enigmatic structures of the vertebrate skeleton. We compare for the first time a) the skeletogenesis sequence of the juvenile stages between short bones such as ulnare and radiale, long bones epiphyses, and sesamoids such as the palmar sesamoid, and b) the shape and dimension of all those structures to identify common traits that allow us to consider them anatomically equivalent. To discard that sesamoids undergo only a mineralization process like the long bone epiphyses of anurans (Ecker, 1889, Haines, 1942; Dickson, 1982; DellOrbo et al., 1992), we include epiphyses in our study.

MATERIALS AND METHODS

Histological and Histochemical Analyses

We analyzed samples of radio-ulna epiphyses, carpals and sesamoids of post-metamorphic specimens of *Leptodactylus bufonius* and *Rhinella arenarum*. We chose these species because they left the aquatic habitat after the metamorphosis and face terrestrial locomotion by two highly different locomotor modes: jumping (*Leptodactylus bufonius*) and walking (*Rhinella arenarum*). The specimens examined belong to the herpetological collection of Fundación Miguel Lillo and are identified as follows: *L. bufonius* (FML 27869, FML 27873, FML 27874, FML 27870, FML 27871, FML 27872, FML 27875, and FML 27876); *R. arenarum* (FML 27877, FML 27878, FML 27879, FML 27880, FML 27881, FML 27882). All specimens were measured with digital calipers (Mitutoyo CD-30C and CD-15B; ±0.01 mm) (Table 1). The size of the specimens was used as a proxy of the development rate of the specimens (Dickson, 1982). However, this criterion should be considered with caution because a direct relationship between age and size has not been proven in anurans (Rozenblut and Ogielska, 2005). The stages of individuals were determined according to the relative percentage of the maximum length, which corresponds to the length of the adult specimen of each studied species (Table 1). Each stage represents a percentage range (±1%) (e.g., stage 2 includes individuals which have a SVL that correspond to the 19–21% of the total length of the adult), thus, some specimens with similar but not identical SVL could be the same stage. The specimens were fixed in a 10% formaldehyde solution for 24 hr. The extracted forelimbs were decalcified with 5% formic acid (5 mL of formic acid, 5 mL of formaldehyde and 100 mL of distilled water) for 1–6 weeks,

TABLE 1. Juvenile's stages according to the relative percentage of the total length of the adult, SVL of *Leptodactylus bufonius*: 51.6–53.6 mm, SVL of *Rhinella arenarum*: 80–100 mm (Cei, 1980)

	Rhinella arenarum	
Stage	SVL (mm)	% Of the total length of the adult
1	17.3	18.21%
2	20.43	21.5%
5	25.75	27.1%
13	41	43.15%
16	47.36	49.85%
28	70.48	74.18%
30	40.9	77.97%
	Leptodactylus bufonius	
14	23.68	45.14%
22	32.32 - 32.92	61.62%– 62.76%
25	35.45	67.58%
29	39.52	75.34%
30	40.9	77.97%
34	45.29	86.34%
35	46.48	88.61%

depending on the sample size. The material was then dehydrated in a graded ethanol series and in *n*-butyl ethanol, and embedded in Histoplast embedding medium. Serial sagittal sections 7-μm thick were cut with a rotary microtome (Microm HM 325) and stained with Mallory trichrome, Hematoxylin-Eosin and alcian blue-periodic acid-Schiff. With the Mallory trichrome technique, the collagen fibers present in the extracellular matrix (ECM) and the fibrocartilage are stained blue and the cellular nucleus and the glycosaminoglycans (keratan sulphate) of the osseous matrix are stained red. The compounds of the cartilage ECM, such as the glycosaminoglycans and proteoglycans, react with basic dyes staining purple with Hematoxylin. The ECM reacts positively with Alcian-Blue because the acid mucins, such as glycosaminoglycans and proteoglycans. A high concentration of neutral mucins, such as collagen fibers, present in the mineralized ECM also reacts positively with the periodic acid-schiff dye, getting a pink coloration (PAS-positive). While the histological techniques show the acidic and basic properties of the tissues, histochemistry involves a chemical and physical reaction that indicates the molecular content of the tissue (Humason, 1962). Histological samples were observed under optical microscopy (Leica ICC 50 HD) and photographed with Nikon Coolpix P6000digital camera. Terminology of digits and carpal osteology follows Fabrezi (1992), and sesamoids terminology follows Ponssa et al. (2010).

Morphometric Analysis

To compare shape among humerus epiphyses, carpals and sesamoids, a contour geometric morphometric analysis was performed. We select the humerus for this analysis because it has only one epiphysis, whereas the radio-ulna presents two fused epiphyses, making the comparison of their shapes not possible. This method is based on the concept that the two figure contours are homologous, and it was initially thought for objects without discrete landmarks (Toro Ibacache et al., 2010). To obtain the contour the dots must be taken around that contour, and must be positioned equidistantly (Toro Ibacache et al., 2010). The digitized dots are adjusted to an *ad-hoc* function, such as harmonics of Fourier analysis, which was recalculated inversely using an eigenvector matrix, letting the score on a particular PC be equal to the mean ± 2 s.d. (standard deviation); finally, the function coefficients are used as components of the shape (Rohlf, 1990). It is known that information about shape is conveyed via the curves of an object boundary lines (Freeman, 1974). We extirpated the humerus, two carpal bones (ulnare and radiale) and two sesamoids (pararadial and palmar sesamoids) of 11 stained and cleared adults *Leptodactylus bufonius* specimens from the Herpetological Collection of Fundación Miguel Lillo (FML-589, FML-672, FML-3568, FML-3868, FML-4366, FML-9779, FML-9780, FML-9782, FML-9783, FML-4908 (two specimens). Radiale and ulnare were selected because, along with element Y, they seem to be highly conservative elements of anuran carpus (Fabrezi and Barg, 2001). Long bones epiphyses, carpal bones and sesamoids were photographed with a Nikon Coolpix P6000 digital camera. The images were previously processed with the software Photoshop to delimit the outline of each bone (i.e., carpals, sesamoids) and the epiphyses of the humerus. We did not consider the size of the bones in this analysis. Each photograph was saved as a bmp image and then processed with the software SHAPE ver. 1.3 (Iwata and Ukai, 2002). This software package evaluates contour shapes based on Elliptic Fourier descriptor (EFDs). EFDs have been effectively applied to the analysis of various biological shapes in animals (Rohlf and Archie, 1984; Ferson et al., 1985; Bierbaum and Ferson, 1986; Diaz et al., 1989; Liu et al., 1996; Laurie et al., 1997) and plants (Yoshioka et al., 2004). The SHAPE software contains four programs: ChainCoder, Chc2Nef, PrinComp and PrinPrint (Iwata and Ukai, 2002). ChainCoder converts a full color image to a binary (black and white) image, reduces noise, traces the contours of objects and describes the contour information as chain-code; Chc2Nef calculates the normalized EFDs from the chain-code information exported by the ChainCoder program. We used the normalization method based on the first harmonics ellipse (20 harmonics), which corresponds to the first Fourier approximation to the contour information; the size and orientation of the contour is standardized according to the size and alignment of the major axis of the ellipse (Iwata and Ukai, 2002). The PrinComp program performs a principal component analysis (PCA) to summarize the information of the Fourier coefficients. Actually, PCA is based on a covariance–variance matrix of the coefficients and not on the correlation matrix. PCA may be used to reduce the dimensionality of the data by analyzing a limited number of PC (principal component) scores of the specimens instead of the original data (Sheets et al., 2006). Finally, we used the PrinPrint program to visualize shape variation. First, the coefficients of the elliptic Fourier descriptors are calculated, letting the score for a particular PC be equal to the mean plus or minus two (± 2) times the standard deviation and the scores of the remaining components be zero. Then the contour shape on each condition can be reconstructed from the coefficients by inverse Fourier transformation. The use of elliptic Fourier descriptors and principal component analysis (EF–PCA) is advantageous because, on the one hand, the method can accurately detect small shape variations and, on other hand, EF–PCA can evaluate the shapes of objects independently of size. This independence is a great advantage because human visual judgment of shape is often misled by size factors.

To detect differences in shape among long bone epiphyses, carpal bones and sesamoids, we performed a MANOVA (homogeneity of slopes test), with the PCs as dependent variables and bones as grouping factor, using the software Statistica (2004).

The three elements studied (epiphysis, carpal and sesamoid) were compared with one-way ANOVA followed by Tukey's test using Infostat software (Di Rienzo et al., 2013). The measurements considered were maximum length and maximum width of five elements of the manus; humerus epiphyses; ulnare and radiale; palmar and pararadial sesamoids. These measurements were taken considering the elements according its physiological position. P values less than 0.05 were considered as significant. Although the definition of short bones considers three dimensions, length, width and height (Ross and Pawlina, 2007), the bidimensional analysis allowed us to gather important data for this study.

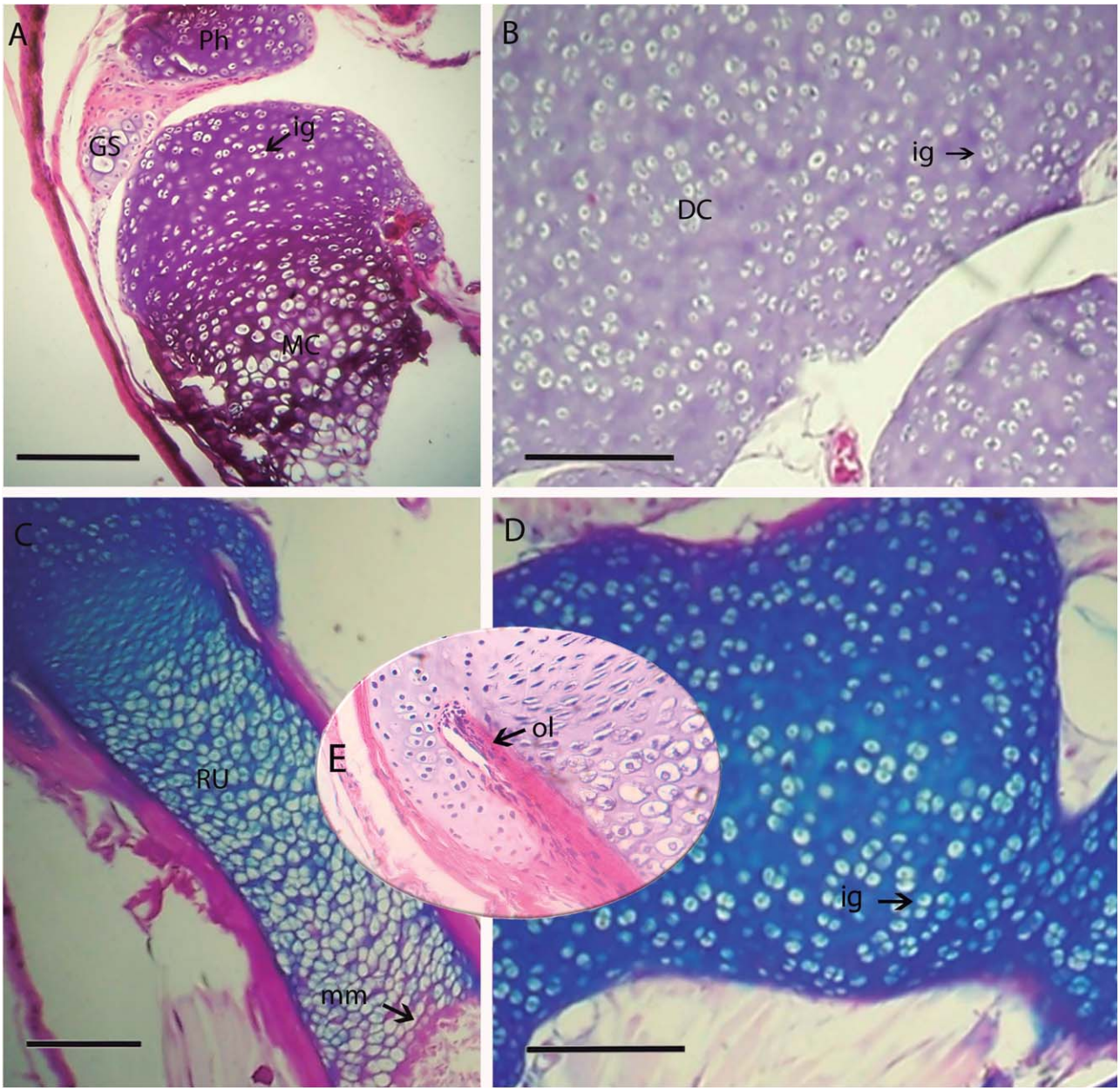

Fig. 1. Stage 5 of *Rhinella arenarum*. **A**: section of Metacarpal V stained with Hematoxylin-Eosin. **B**: section of Distal carpal 5 + 4+3 stained with Hematoxylin-Eosin. **C**: section of radio-ulna stained with alcian blue-periodic acid-schiff. **D**: section of Distal carpal 5 + 4+3 stained with alcian blue-periodic acid-schiff. **E**: detail of section of lateral articular cartilage of the epiphyses of radio-ulna stained with Hematoxylin-Eosin. (DC) Distal carpal, (MC) metacarpal, (GS) glide sesamoid, (Ph) phalange, (RU) radio-ulna, (ig) isogen groups, (ol) osteochondral ligament, (mm) mineralized matrix. Scale bar 200 μm.

RESULTS

Histological and Histochemical Analyses

The histological analysis showed that the evaluated bones (radio-ulna, carpals, and sesamoids) underwent chondral (perichondral and endochondral) ossification process. This technique helped us both to determine the timing of ossification during postmetamorphic stages and to compare the elements (long bones epiphyses, carpals and sesamoids) among them and between the two analyzed species. The stages with the most relevant changes are described below.

Rhinella arenarum

Stages 1, 2, and 5 (Fig. 1): In the epiphyses of long bones and carpals, a cartilaginous ECM with isogenous groups is visible (Fig. 1A,B,D). The ECM stains blue with Hematoxylin-Eosin, suggesting a high concentration of glycosaminoglycans and proteoglycans (Fig. 1A–

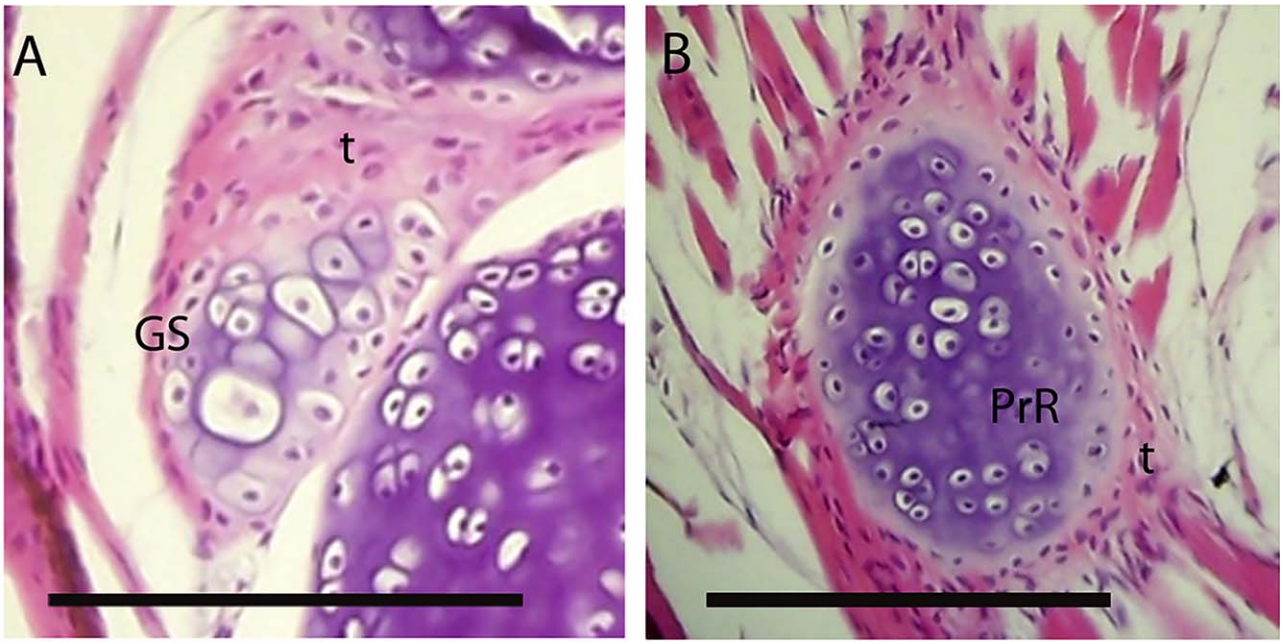

Fig. 2. Stage 5 of *Rhinella arenarum*. **A**: section of glide sesamoid between metacarpal and phalange IV stained with Hematoxylin-Eosin. **B**: section of pararadial stained with Hematoxylin-Eosin. (GS) glide sesamoid, (PrR) pararadial sesamoid, (t) tendon. Scale bar 200 μm.

C). The radio-ulna diaphyses show the growth cartilage with its characteristic zones (Fig. 1C). In Stage 5, the diaphyses of radio-ulna show mineralization in the ECM of the hypertrophic zone of the growth cartilage (Fig. 1C). A detail of the lateral articular cartilage of the radio-ulna epiphyses, and the osteochondral ligament with its collagens fibers, which run parallel to the bone axis, is shown in Fig. 1E. A glide sesamoid between the phalange and the metacarpal of digit IV (Fig. 2A), and the pararadial sesamoid between the ulnare and ulna (Fig. 2B) show hypertrophic chondrocytes; they are immersed in a tendinous tissue.

Stage 13 (Fig. 3): In the epiphysis of the phalange of digit IV, the lateral articular cartilage is still not fully formed. The diaphyses of this phalanx exhibit the growth cartilage and osteocytes within the marrow cavity (Fig. 3A). In the joint between metacarpal II and phalanx of digit II, the collagen fibers of the immature ligaments show abundant nuclei (Fig. 3B). Carpals show no major changes. A glide sesamoid, which is visible as fibrocartilaginous tissue, is conspicuous on one side of this joint (Fig. 3B).

Stage 16 (Fig. 4): In the long bones, the diaphyses of the metacarpal II display endochondral trabeculae (Fig. 4A). Carpals continue without major changes. The pararadial sesamoid of fibrocartilage is visible between the ulna and the ulnare (Fig. 4B). Fibrocartilaginous tissue is also evident in the menisci (Fig. 4A).

Stage 28 (Fig. 5): Both the diaphyses of long bones and carpals (radiale and the distal carpal 3 + 4+5) show endonchondral ossification (Fig. 5A,B,D,E). The carpals present a small marrow cavity with cartilaginous spicules, osteoblast and trabeculae of endochondral bone (Fig. 5B,E); the presence of abundant erythrocytes inside the blood vessels is also noticeable (Fig. 5E). The palmar sesamoid shows a cartilaginous ECM with isogen groups. This sesamoid is surrounded by tendinous tissue (Fig. 5C,F).

Leptodactylus bufonius

Stage 14 (Fig. 6A,B): The radio-ulna diaphyses and the core of the carpals show hypertrophic chondrocytes that area arranged concentrically. A myotendinous junction is distinguishable between the radio-ulna epiphyses and the *pronator quadratus* (Fig. 6D). In the cartilage ECM of the long bone epiphyses, the presence of negative sulfate groups is evident (Fig. 6C). In the epiphyseal cartilage of radio-ulna, the articular cartilage, lateral articular cartilage and growth cartilage are observed (Fig. 6C); a thin layer of immature tendon with many nucleus is evident around the radiale (Fig. 6B).

Stage 22 (Figs. 7 and 8): The long bone diaphyses and carpals show an increment of the medular cavity size and cartilage spicules (Fig. 7A,B; 8A, C, E). In one specimen, the ECM is mineralized, as shown by the high collagen concentration around the isogen groups and the hypertrophic chondrocytes in diaphysis and epiphysis (Fig. 7D,E). Other specimens do not show mineralization in the matrix of the metacarpal III (Fig. 8B,D,F). Hyaline cartilage of the developing palmar sesamoid emerges from a fibrocartilaginous transition area into the tendinous tissue (Fig. 7C).

Stage 25 (Fig. 9): Endochondral bone trabeculae appear in the medular cavity of both long bone diaphyses and carpals, but not in the epiphyses of long bone. The ECM stains blue with Hematoxylin-Eosin, suggesting a high concentration of proteoglycans and is not mineralized. Abundant collagen is evident in the bone trabeculae and bone edges.

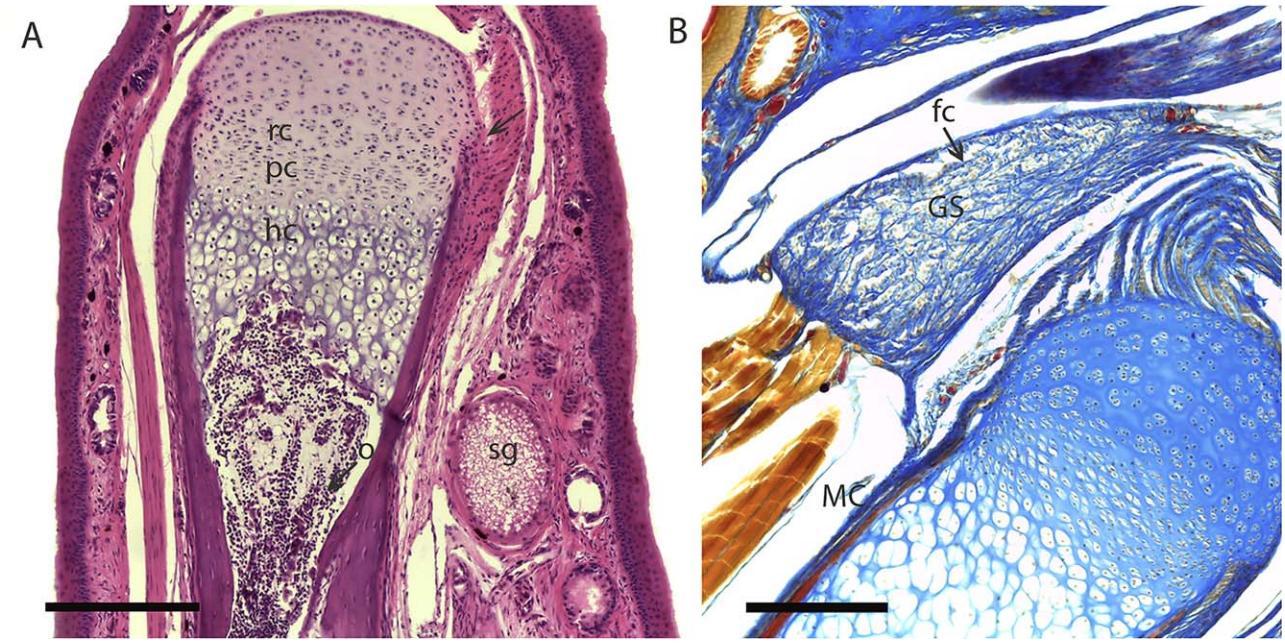

Fig. 3. Stage 13 of *Rhinella arenarum*. **A**: section of phalange IV stained with Hematoxylin-Eosin, the cartilage growth zones are noticeable. **B**: section of metacarpal II stained with Mallory trichrome, a fibrocartilage tissue is noticeable. (fc) fibrocartilage, (GS) glide sesamoid, (hc) hypertrophic chondrocyte zone (o) osteocytes, (MC) metacarpal, (pc) proliferation cartilage zone, (rc) reserve cartilage zone, (sg) serous gland. Scale bar 200 μm.

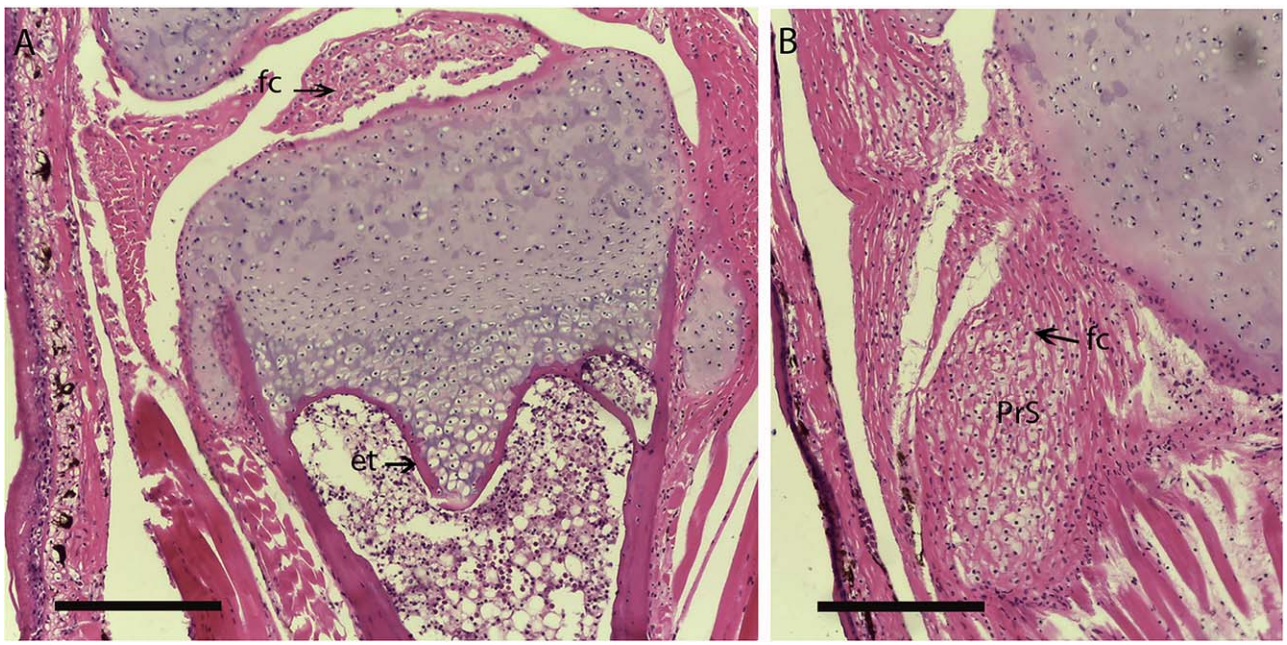

Fig. 4. Stage 16 of *Rhinella arenarum*. **A**: section of metacarpal II stained with Hematoxylin-Eosin. **B**: section of fibrocartilaginous tissue stained with Hematoxylin-Eosin. (PrR) pararadial sesamoid, (et) endochondral trabeculae, (fc) fibrocartilaginous tissue. Scale bar 200 μm.

Stage 29 (Fig. 10): The trabeculae of endochondral bones and an increased size of the marrow cavity in the long bone diaphyses and carpals are evident (Fig. 10A, B). The ECM of the cartilage in the epiphyses of the long bones and in diaphyses is mineralized (Fig. 10D, E). A large amount of osteocytes and blood vessels with

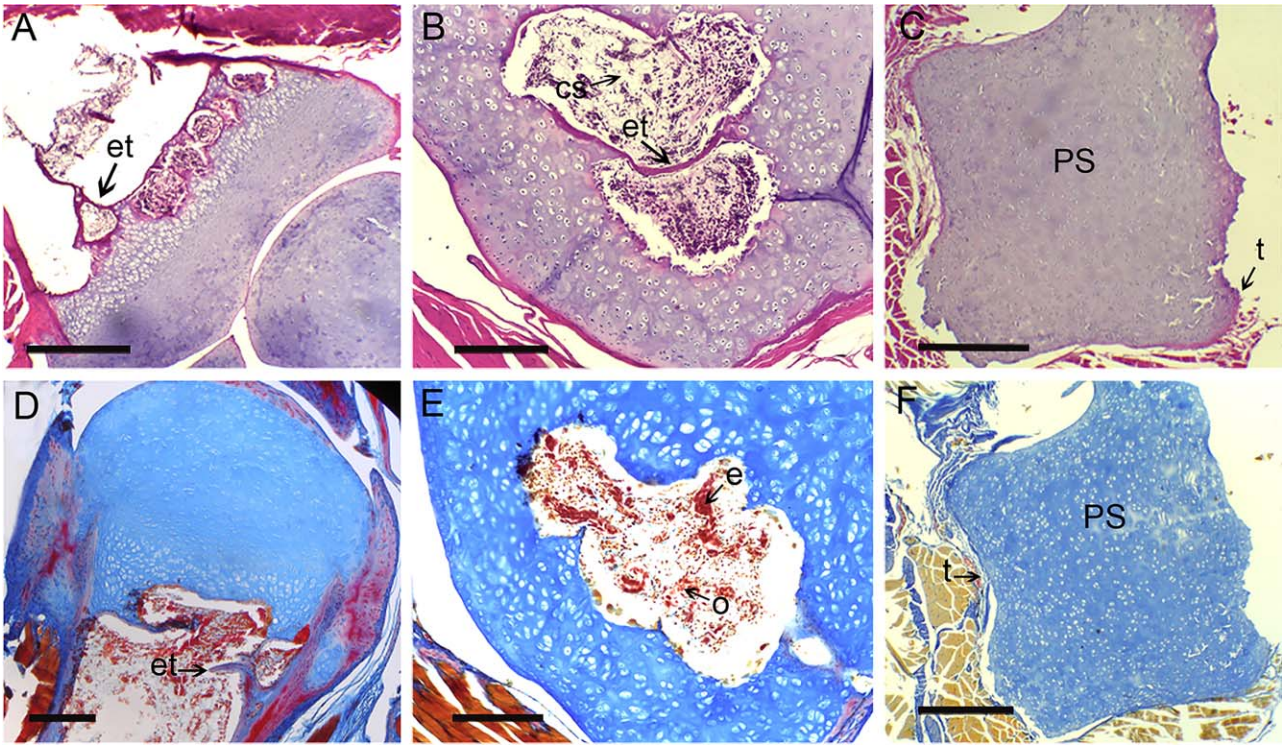

Fig. 5. Stage 28 of *Rhinella arenarum*. **A**: section of metacarpal II stained with Hematoxylin-Eosin. **B**: section of Y element stained with Hematoxylin-Eosin. **C**: section of palmar sesamoid stained with Hematoxylin-Eosin. **D**: section of metacarpal II stained with Mallory trichrome. **E**: section of Y element stained with Mallory trichrome. **D**: section of palmar sesamoid stained with Mallory trichrome. (cs) cartilage spicules, (e) erythrocytes, (et) endochondral trabeculae, (o) osteocytes, (PS) palmar sesamoid, (t) tendon. Scale bar 200 μm.

erythrocytes is evident in the marrow cavity in both carpal and diaphyses of the long bones (Fig. 10G). The palmar sesamoid is cartilaginous, and a fibrocartilaginous transition between this sesamoid and its tendon is visible (Fig. 10C). The fibers of the osteochondral ligament (Felisbino and Carvalho, 2000) are visible (Fig. 10F).

Stage 30 (Fig. 11): The trabeculae of endochondral bones in long bones diaphyses and carpals (Fig. 11D) are conspicuous. In the epiphyses, the osteochondral ligament (Felisbino and Carvalho, 2000) between the periosteal bone and the lateral articular cartilage is evident (Fig. 11A). The joint capsule is formed by dense fibrous connective tissue that adheres firmly to the bones via the attachment-zone tendinous-cartilage (Fig. 11A). The carpal bone ulnar is rounded by tendinous tissue (Fig. 11B).

Stage 34 (Fig. 12) and Stage 35: Diaphyses of long bones, carpals and palmar sesamoid show a bigger marrow cavity and even more endochondral trabeculae than in the previous stages (Fig. 12A, B, C, F). In the specimen in Stage 34, the tendinous tissue surrounding the ulnare is evident (Fig. 12B). The osseous matrix shows considerable amount of keratin sulphate (Fig. 12D, E); this is noticeable in the endochondral trabeculae, which stains red. A big amount of osteocytes and blood vessels with erythrocytes are evident in the marrow cavity in carpals (Fig. 12D, E).

Morphometric Analysis

The PCA of the bone data set (N = 51) of the contour morphometric geometric analysis is shown in the scatter plot of the first and second principal components (PC1 vs. PC2; Fig. 13). PC1 and PC2 captured 43.28% and 20.02% of the total shape variation, respectively, and together with PC3 accounted for 72.29%; the remaining percentages are listed in Appendix . The effects of each PC on bone (epiphyses, carpal, and sesamoid) shape are visualized in the Fig. 14. These reconstructed shapes indicate that the first PC described shape change associated with an enlargement of the maximum longitudinal diameter, this expansion being stronger in the left portion of the element. On PC2, shape variation was determined by expansion in the extreme sides, which gave a triangular configuration to both extreme shapes, with the more expanded sides in opposite areas (above and below) of the variation.

The PCA of the contour morphometric variables of the five osteological elements shows a clear separation through PC1 of a group composed of the radiale, whereas PC2 separated a cluster of the epiphyses, and a group formed by the sesamoids (palmar and pararadial) and the ulnare. The MANOVA shows significant differences among bones (Wilk's λ $F_{12,19}$=0.05, $P < 0.000$). Subsequent univariate F-test showed that this difference was significant for each principal component (PC1, PC2 and PC3) (Table 2). Bone–bone comparisons (Table 3) show that the shape of radiale significantly differed from those of paradial sesamoid, palmar sesamoid, ulnare, and epiphyses of humerus ($P < 0.00$).

The ANOVA including the length and the width of the five elements of the manus revealed a significant

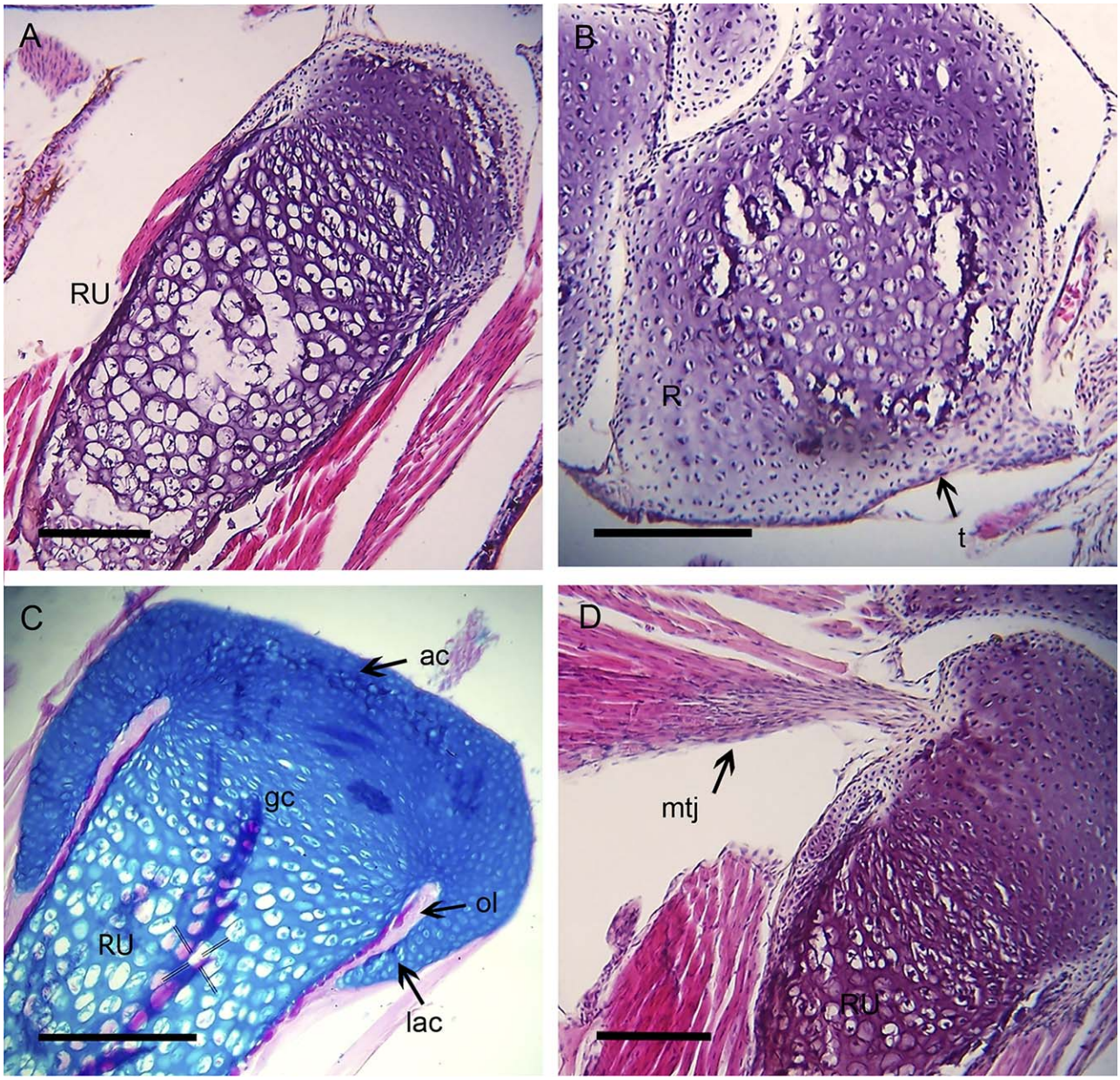

Fig. 6. Stage 14 of *Leptodactylus bufonius*. **A**: section of radio-ulna stained with Hematoxylin-Eosin. **B**: section of radial stained with Hematoxylin-Eosin. **C**: section of radio-ulna stained with alcian blue-periodic acid-schiff. **D**: section of radio-ulna and the myo-tendinous junction stained with Hematoxylin-Eosin. (ac) articular cartilage, (gc) growth cartilage, (lac) lateral articular cartilage, (mtj) myo-tendinous junction, (ol) osteochondral ligament, (RU) radio-ulna, (R) radial, (t) tendon. Scale bar 200 μm.

difference ($P < 0.05$) in all the elements, except for the radiale bone ($P = 0.64$) (Table 4).

DISCUSSION

Of the three analyzed aspects (skeletogenesis, shape and proportions of sesamoids), skeletogenesis is clearly a shared configuration between carpal bones and sesamoids. Even when the ossification process shows an important difference in sesamoids—the appearance of fibrocartilage in the transition between the tendon and the hyaline cartilage during their development—both structures present the same pattern of endochondral ossification. It should be considered however, that sesamoids exhibit a pervasive relationship with tendons that has not been described in carpal bones or long bones epiphyses. With regard to sesamoid shape and dimensions, our data indicate that bones categorization based on these aspects-particularly those that stay that short bones are those having their three dimensions equally developed (Ross and Pawlina, 2007) is vague and therefore is ineffective to classify the skeletal bones.

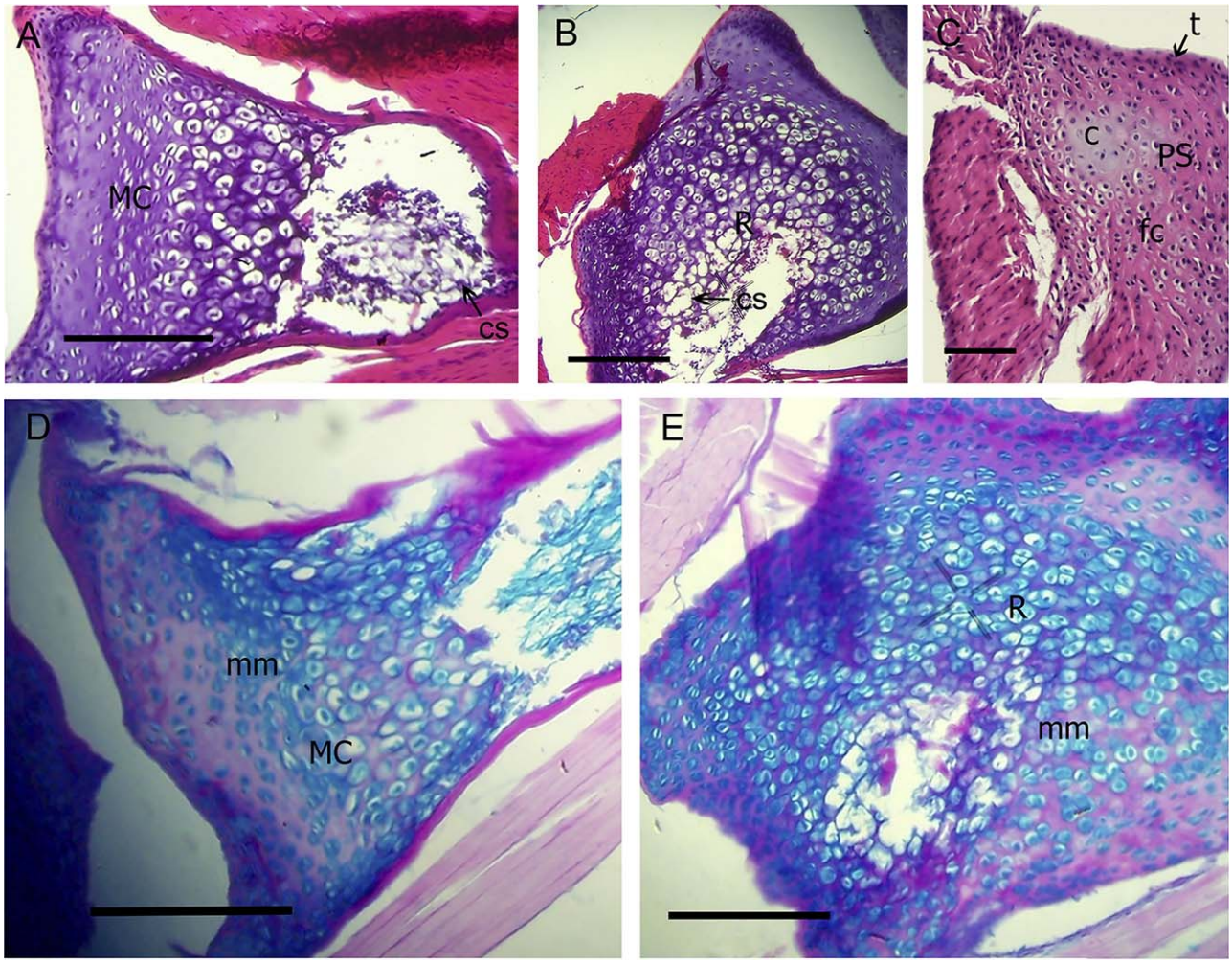

Fig. 7. Stage 22 of *Leptodactylus bufonius* (specimen FML 27873; SVL 32.32mm) **A**: section of metacarpal IV stained with Hematoxylin-Eosin. **B**: section of radial stained with Hematoxylin-Eosin. **C**: section of palmar sesamoid stained with Hematoxylin-Eosin. **D**: section of metacarpal IV stained with alcian blue-periodic acid-schiff. **E**: section of radial stained with alcian blue-periodic acid-schiff. (c) cartilage, (cs) cartilage spicules, (fc) fibrocartilage, (MC) metacarpal, (mm) mineralized matrix, (PS) palmar sesamoid, (R) radial, (t) tendon. Scale bar 200 μm.

Histological and Histochemical Analyses

The sequence of skeletogenesis shows that all three structures (epiphyses, carpals and sesamoids) undergo a cartilaginous and a mineralized phase in their development. Only sesamoid and carpal bones exhibit endochondral ossification. Finally, only sesamoids show fibrocartilaginous tissue (Table 5), although it was detected using unspecific techniques. Perichondral and endochondral ossification is evident from the first examined juvenile stages in carpal bones and sesamoids, which previously go over a mineralized stage (Table 5). Sarin and Carter (2000) mentioned that most of sesamoids develop by endochondral ossification, similarly to long bones and following the same chondrogenic and osteogenic pathways. In most anurans, however, the epiphyses show a mineralized matrix, which never ossified (Haines, 1940; Felisbino and Carvalho, 1999), making the comparison among these structures less straightforward. This lack of endochondral ossification is a fundamental difference with the epiphysis of birds and mammals; although, Dickson (1982) reported a reduced endochondral bone in older individuals of *Rana temporaria*, and DellOrbo et al. (1992) for *Rana esculenta*.

It has been demonstrated that the collagen molecules act as templates for mineral deposition (Landis et al., 1996; Landis and Silver, 2002; Doherty, 2010; Bonucci and Gomez, 2012). Thus, mineralization can be inferred by the increase of the areas stained in pink in the cartilage ECM, which indicate an increase in the collagen secretion. All three studied structures: long bone epiphyses, carpal bones, and sesamoids, go through a mineralization stage. Our data allow us to infer calcium deposits because the heterogeneity of the histochemistry staining of the ECM of long bones epiphyses and carpal bones. Some cartilaginous areas presented high concentration of glycosaminoglycans, with the mineralized areas exhibiting an increment of collagen fibers, and a deposition of calcium salts. However, the mineralization process not always is a previous step to the ossification process. In *L. bufonius*, there is an apparently variable pattern.

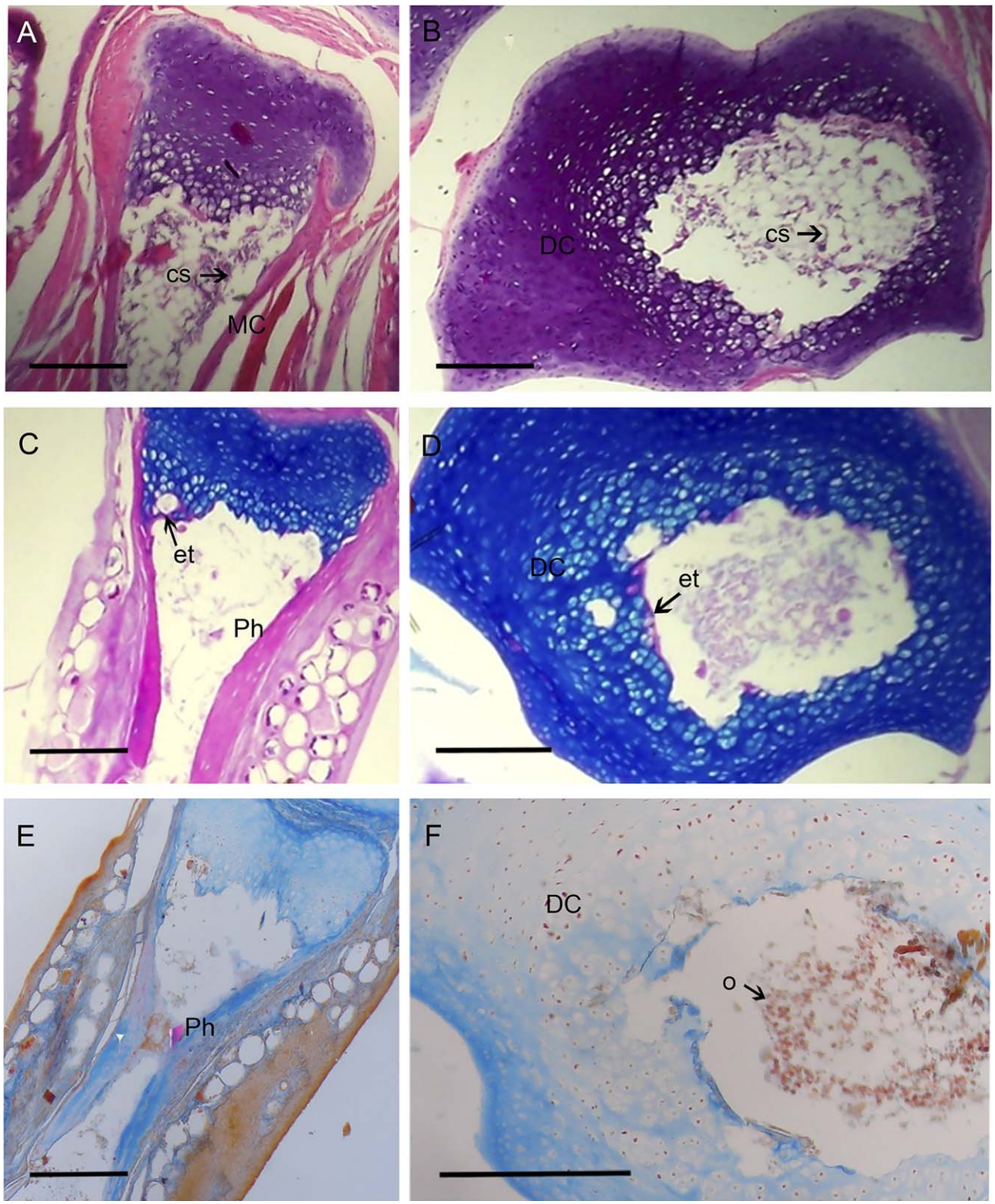

Fig. 8. Stage 22 of *Leptodactylus bufonius* (specimen FML 27874, SVL 32.92mm). **A**: section of metacarpal III stained with Hematoxylin-Eosin. **B**: section of distal carpal 5 + 4+3 stained with Hematoxylin-Eosin. **C**: section of phalange III stained with alcian blue-periodic acid-schiff. **D**: section of distal carpal 5 + 4+3 stained with Mallory trichrome. **E**: section of phalange III stained with Mallory trichrome. **F**: section of distal carpal 5 + 4+3 stained with Mallory trichrome. (cs) cartilage spicules, (DC) distal carpal, (et) endochondral trabeculae, (MC) metacarpal, (o) osteocytes, (Ph) phalange. Scale bar 200 μm.

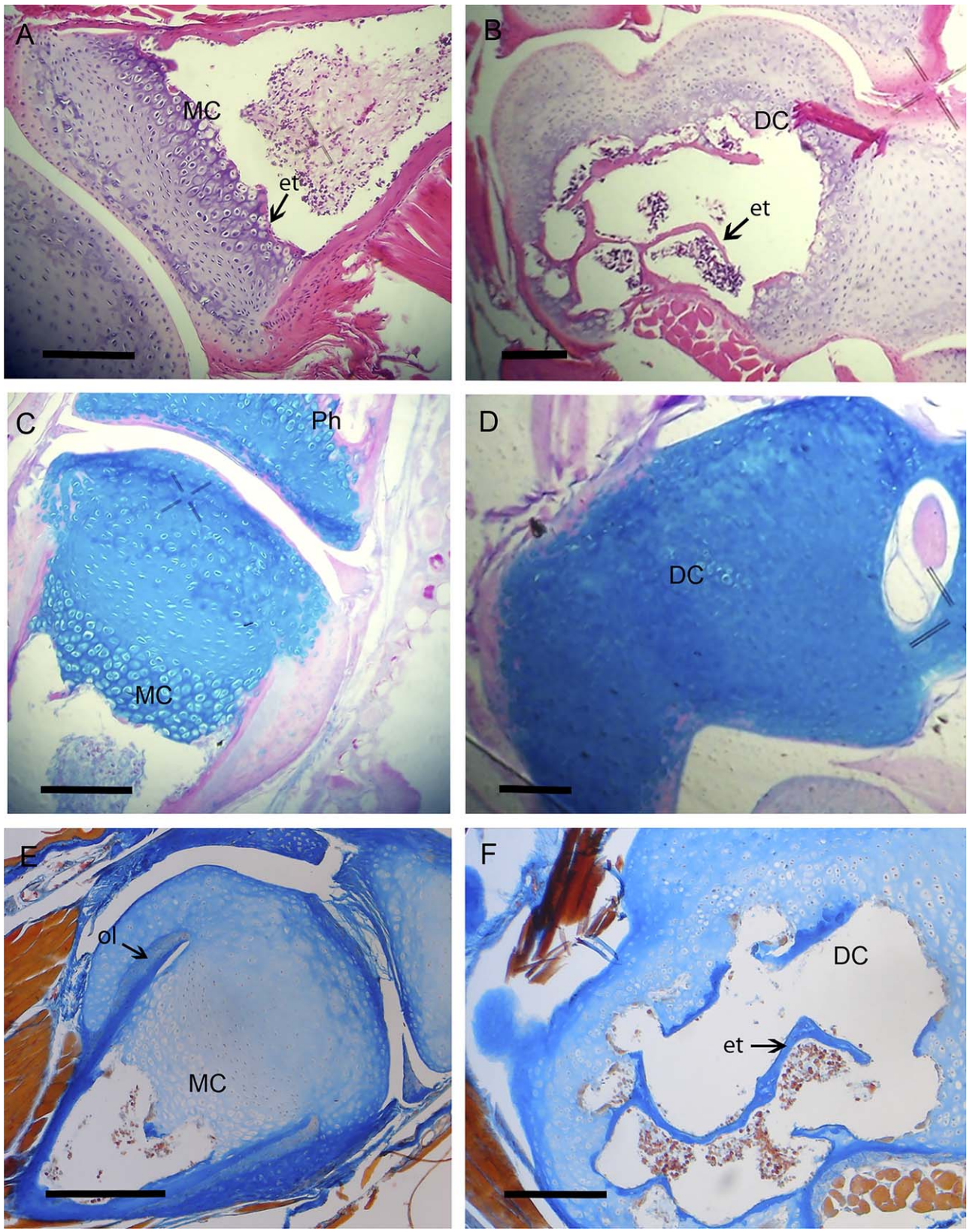

Fig. 9. Stage 25 of *Leptodactylus bufonius*. **A**: section of metacarpal III stained with Hematoxylin-Eosin. **B**: section of distal carpal 5 + 4+3 stained with Hematoxylin-Eosin. **C**: section of metacarpal and phalange IV stained with alcian blue-periodic acid-schiff. **D**: section of distal carpal 5 + 4+3 stained with alcian blue-periodic acid-schiff. **E**: section of metacarpal II stained with Mallory trichrome. **F**: section of distal carpal 5 + 4+3 with Mallory trichrome. (DC) distal carpal, (et) endochondral trabeculae, (MC) metacarpal, (ol) ostochondral ligament (Ph) phalange. Scale bar 200 μm.

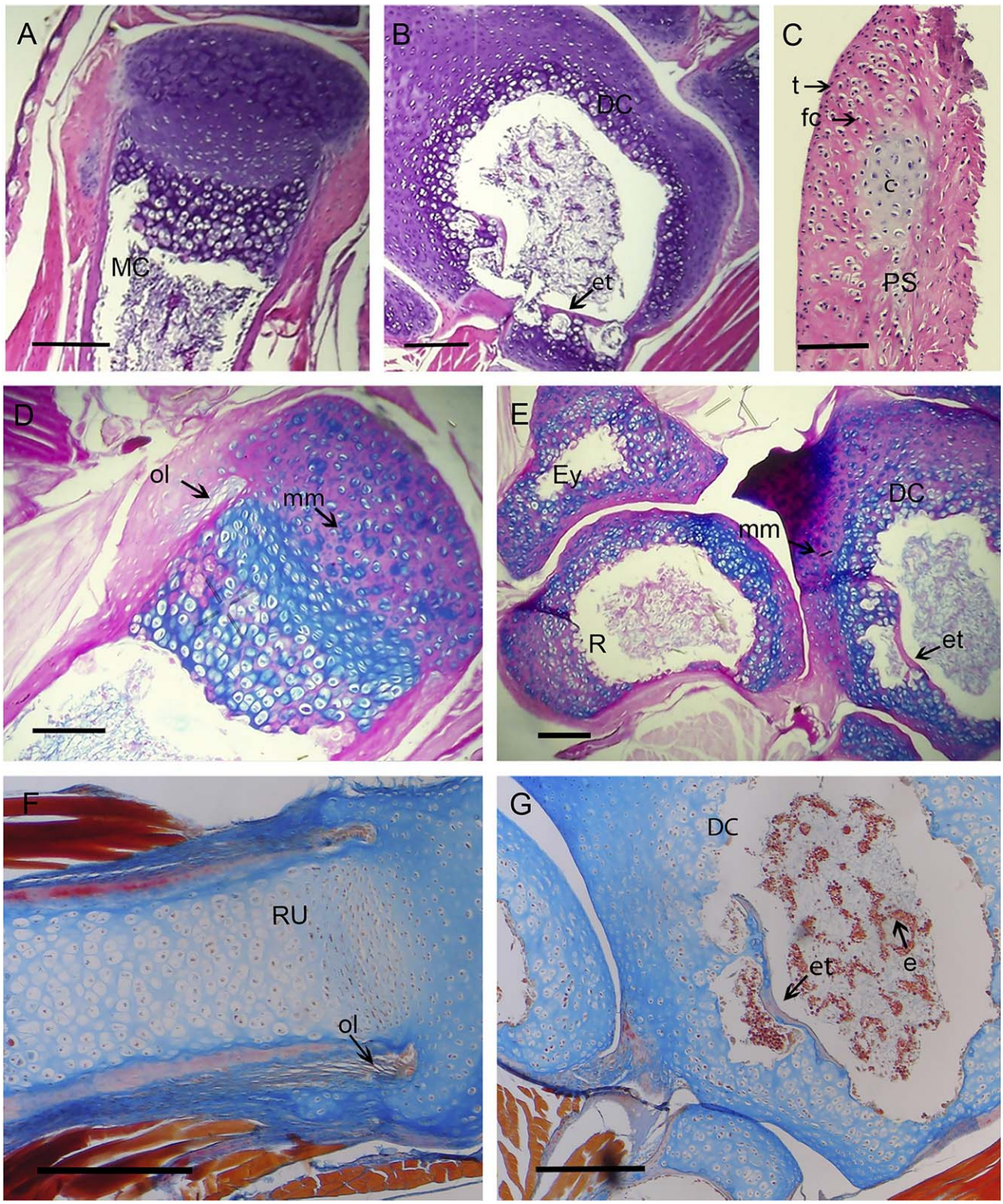

Fig. 10. Stage 29 of *Leptodactylus bufonius*. **A**: section of metacarpal IV stained with Hematoxylin-Eosin. **B**: section of distal carpal 5 + 4+3 stained with Hematoxylin-Eosin. **C**: section of palmar sesamoid stained with Hematoxylin-Eosin. **D**: section of metacarpal IV stained with alcian blue-periodic acid-schiff. **E**: section of distal carpal 5 + 4+3 stained with alcian blue-periodic acid-schiff. **F**: section of radio-ulna stained with Mallory trichrome. **G**: section of distal carpal 5 + 4+3 stained with Mallory trichrome. (c) cartilage, (DC) distal carpal, (e) erythrocytes, (et) endochondral trabeculae, (Ey) Y element, (fc) fibrocartilage, (MC) metacarpal, (ol) osteochondral ligament, (PS) palmar sesamoid, (R) radial, (RU) radio-ulna, (mm) mineralized matrix, (t) tendon. Scale bar 200 μm.

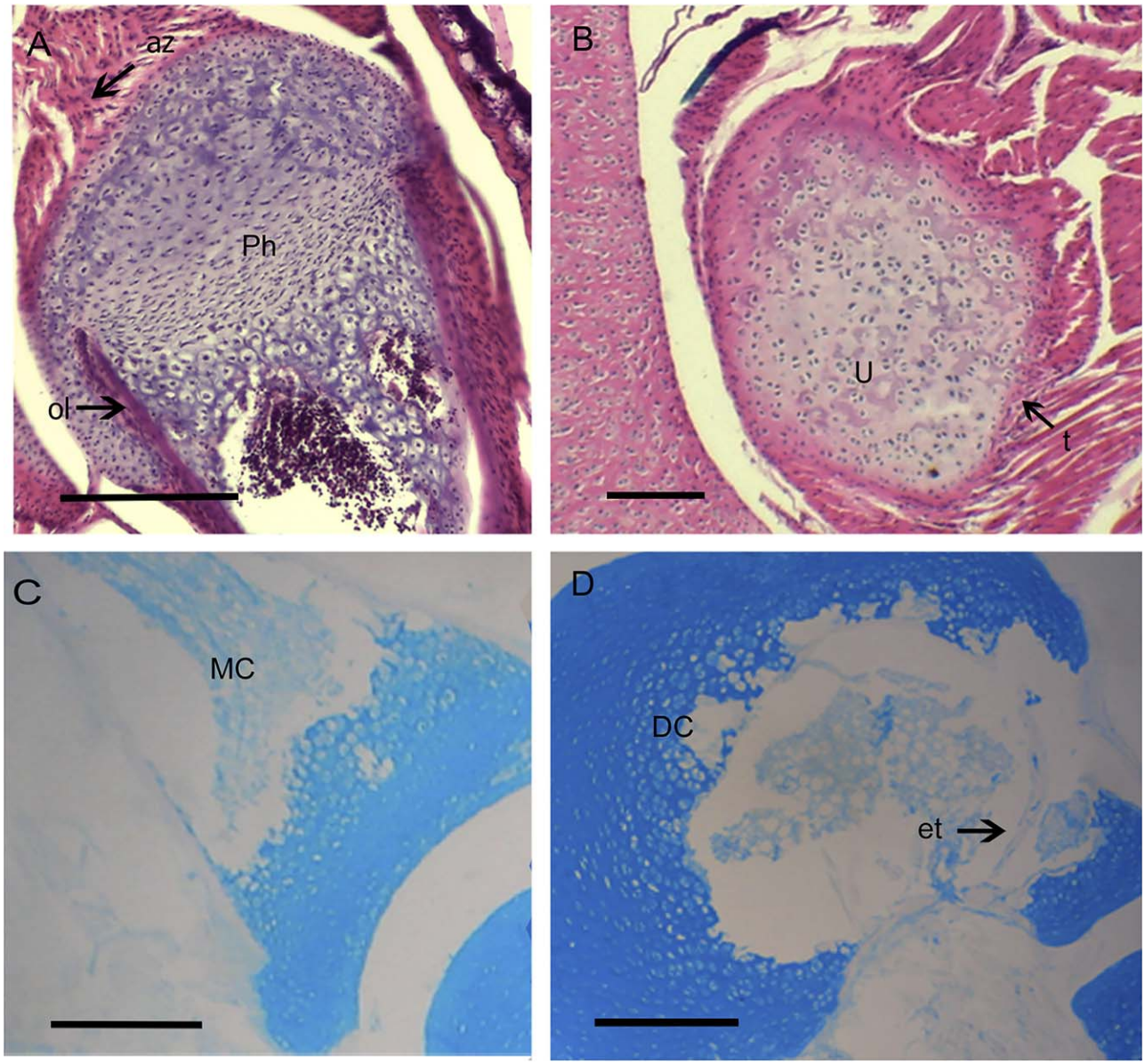

Fig. 11. Stage 30 of *Leptodactylus bufonius*. **A**: section of phalange IV stained with Hematoxylin-Eosin. **B**: section of ulnar stained with Hematoxylin-Eosin. **C**: section of metacarpal IV stained with alcian blue-periodic acid-schiff. **D**: section of distal carpal 5 + 4+3 stained with alcian blue-periodic acid-schiff. (az) attachment-zone fibrocartilage, (DC) distal carpal, (et) endochondral trabeculae, (MC) metacarpal, (ol) osteochondral ligament, (Ph) phalange, (t) tendon, (U) ulnar. Scale bar 200 μm.

Specimens in Stages 22 (Fig. 9) and 29 (Fig. 12) showed a mineralized matrix in their carpal bones before bone trabeculae formation; whereas other specimens of Stages 22 and Stage 25 showed a cartilaginous matrix first, and then bone trabeculae; and a stage of mineralization was not observed. Felisbino and Carvalho (2001) stressed that the formation of bone trabeculae is not dependent on cartilage mineralization, since osteoblast can deposit bone on the surface of unmineralized cartilage. Our findings in *L. bufonius* supports the idea of Felisbino and Carvalho (2001) regarding the lack of spatial or temporal association with calcium deposition and trabeculae formation; accordingly, many events occurring during endochondral ossification are not necessarily related to each other. Matrix mineralization could be explained as a consequence of epigenetic factors acting on each individual; that is, some specimens could be subjected to higher mechanical force in their lives than others (Van't Veen et al., 1995). Thus, matrix mineralization in *Rana catesbeiana* is variable, and occurs as a reinforcement event of bones in adulthood (Felisbino and Carvalho, 2001); whether this is the case in the species here studied remain as an open question.

The sequence of mineralization and ossification processes is equivalent in long bones epiphyses, carpals and sesamoids, although their timing is not synchronic.

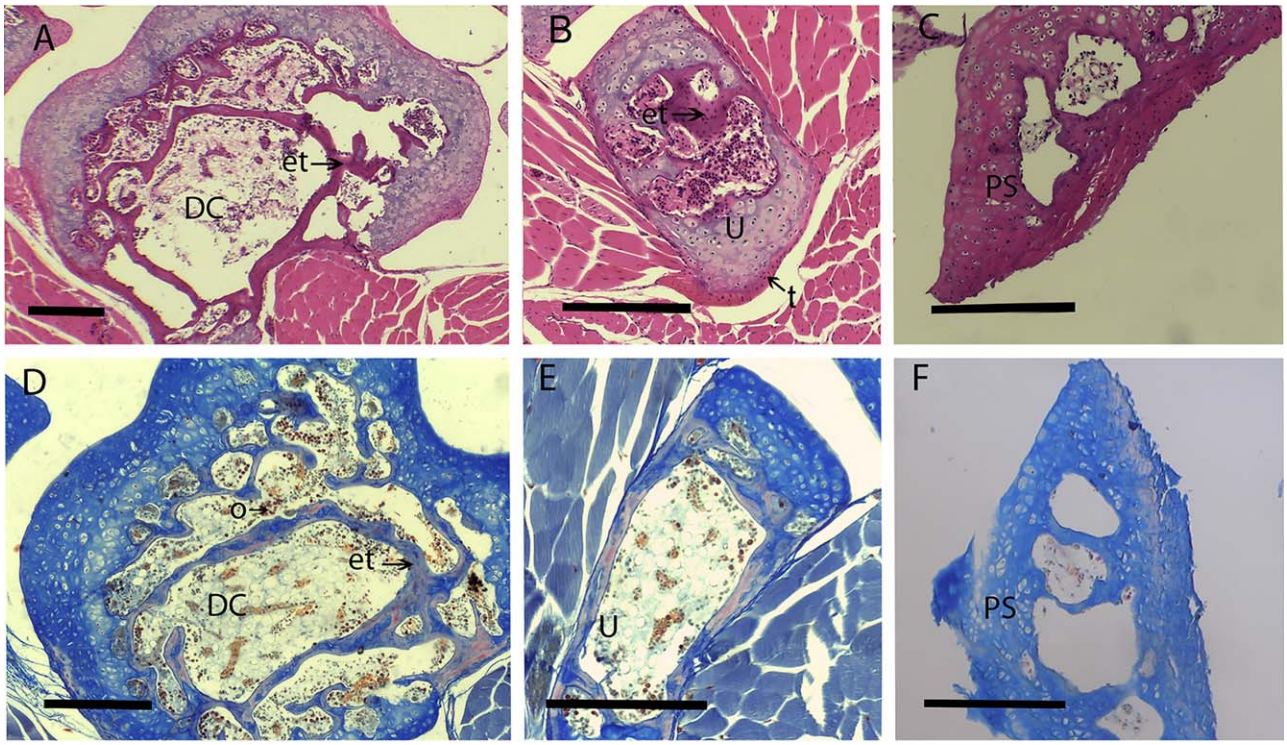

Fig. 12. Stage 34 of *Leptodactylus bufonius*. **A**: section of distal carpal 5 + 4+3 stained with Hematoxylin-Eosin. **B**: section of ulnar stained with Hematoxylin-Eosin. **C** section of palmar sesamoid stained with Hematoxylin-Eosin. **D**: section of distal carpal 5 + 4+3 stained with Mallory trichrome. **E**: section of ulnar stained with Mallory trichrome. **F**: section of palmar sesamoid stained with Mallory trichrome. (DC) distal carpal, (et) endochondral trabeculae, (o) osteocytes, (PS) palmar sesamoid, (t) tendón, (U) ulnar. Scale bar 200 μm.

Thus, in one specimen (*L. bufonius* Stage 25, SVL 35.45 mm), the carpal bones showed bone trabeculae in the marrow cavity, whereas sesamoids exhibited incipient endochondral trabeculae only in bigger specimens (Stage 34, SVL 45.29 mm). Similarly, in *Rhinella arenarum* the carpal bones and sesamoids were cartilaginous in all the observed specimens, except in the biggest one. This specimen showed carpal bones with endochondral ossifications but the palmar sesamoid was still cartilaginous. On the contrary, the long bones epiphyses of both species did not ossify even in adults specimens, which is in agreement with previous findings (Ecker, 1889; Hinchliffe and Johnson, 1983; Duellman and Trueb; 1994; Felisbino and Carvalho, 2002; Vera and Ponssa, 2014). Ossification process in long bone diaphyses started earlier than in carpal bones and sesamoids. Our data indicate that the epiphyses of long bones exhibit a common trajectory with short bones and sesamoids; then, the epiphyses arrested their skeletogenesis process, remaining in the phase of mineralization, whereas the other elements continued to develop until ossification is complete.

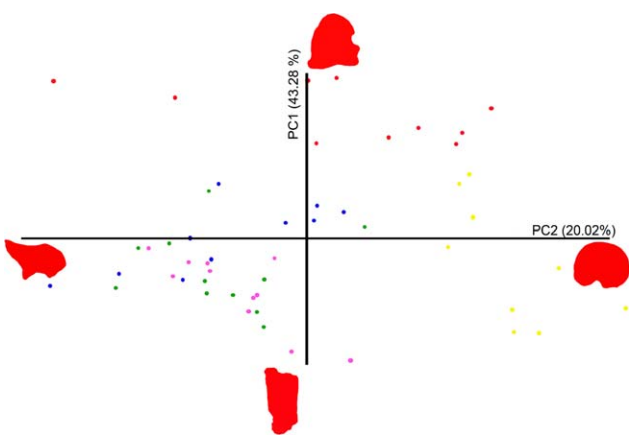

Fig. 13. Principal component analysis. The percentage of variance explained by each of the axes is indicated. Red dots: radial; green dots: pararadial sesamoid; purple dots: palmar sesamoid; blue dots: ulnar; yellow dots: epiphyses. The red figures represents some of the elements; radial and palmar on the positive and negative Y axe, respectively; epiphyses and ulnar the negative Y axe there is palmar, on the positive and negative X axe, respectively.

Of the three elements analyzed, only the sesamoids showed a fibrocartilaginous configuration recognizable in the glide sesamoid located adjacent to the joint between the metacarpal and the first phalange of digit IV, in the pararadial sesamoid, and in the palmar sesamoid. Sesamoid fibrocartilage was also reported in the proximal interphalangeal joints of the finger and toes in humans, specifically on the extensor tendon (Benjamin et al., 1993; Lewis et al., 1998; Benjamin and Ralphs, 1998); on the deep surface of the Achilles tendon of mammals (Rufai et al., 1992, 1995); in the suprapatella, which lies proximal to the patella and forms an

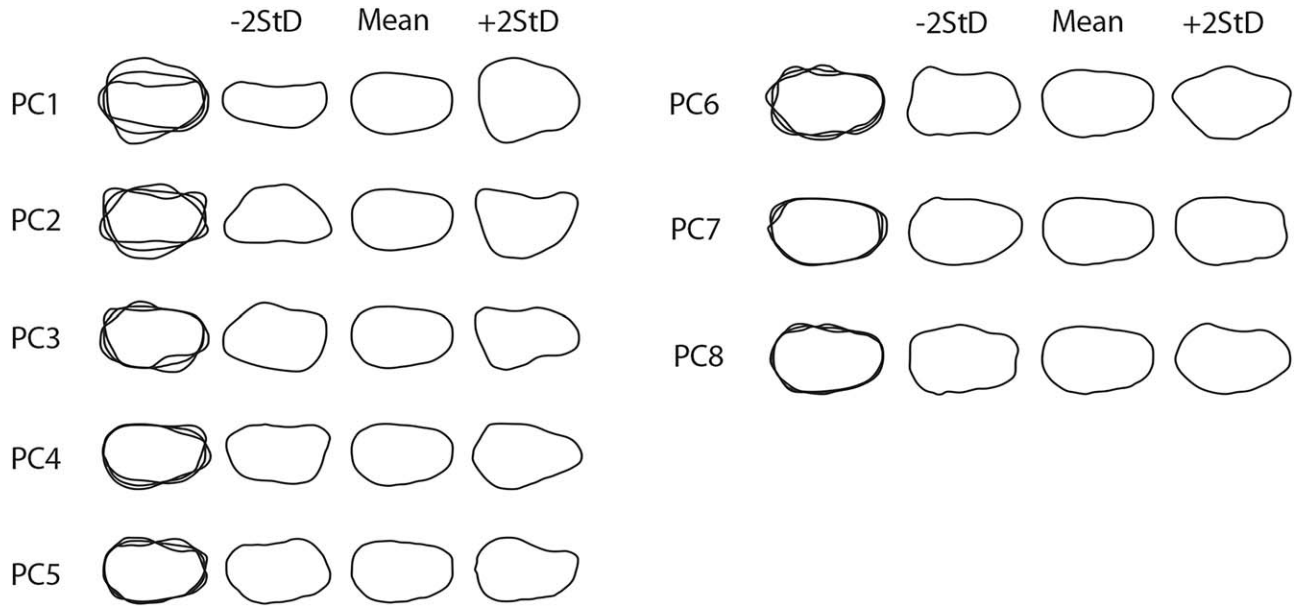

Fig. 14. Effects of each principal component on bones (sesamoid, carpal, and epiphyses). Each column shows the case where the scores takes -2s.d (standard deviation), mean, or +2 s.d., the left-hand column shows the overlaid drawings of the three cases.

TABLE 2. Univariate Results of MANOVA for each principal component (PC)

	F	*P*
PC1	27.63	0.00
PC2	19.60	0.00
PC3	2.76	0.03

Low values of *p* show that difference among bones is significant for each principal component.

TABLE 3. Bonferroni post hoc test results of the MANOVA test, showing the comparison between pair of bones

	Radial	Paradial	Palmar	Ulnar
Epiphysis	**0.00**	1.00	1.00	0.73
Ulnar	**0.00**	1.00	0.05	
Palmar	**0.00**	1.00		
Pararadial	**0.00**			

P values indicating significant differences are in bold.

TABLE 4. ANOVA Tukey test showing mean values, *F*-scores and their *P*-values of length and width measurements for four elements (long bone epiphyses, radial, ulnar, palmar, and pararadial sesamoids)

	$\bar{X}$	F	*P*	d.g
Epiphyses		36.05	< 0.0001	1
Length	3.35			
Width	2.36			
Radial		0.22	0.6415*	1
Length	1.70			
Width	1.63			
Ulnar		19.61	0.0003	1
Length	2.35			
Width	1.66			
Palmar sesamoid		113.14	< 0.0001	1
Length	2.05			
Width	1.18			
Pararadial sesamoid		9.44	0.0066	1
Length	0.59			
Width	0.43			

d.g: degrees of freedom. *Non-significant *P*-value.

extension of the articular surface (Ralphs and Benjamin, 1994), and in the patella of *Gallus gallus* (Vickaryous and Olson, 2007). A fibrocartilaginous tissue has been reported also in the capsule of the same joint (Ralphs and Benjamin, 1994; this work). The presence of a fibrocartilaginous tissue in such a diversity of tetrapod taxa suggests that it must be part of the normal sequence in the sesamoid development. However, there are papers about sesamoid development without mentions to a fibrocartilage stage (Ponssa et al., 2010) this is probably because they are focused on too early stages. The fibrocartilaginous matrix originates as a modification of the ECM of tendon or ligaments at sites where these elements are under compression (Ralphs and Benjamin, 1994, 1998). Our data show that in the structure of the fibrocartilage there is a continuum spectrum of tissues between dense fibrous connective tissue and hyaline cartilage (see also Ralphs and Benjamin, 1994). The fibrocartilage cells are interwoven collagen fibers or lie in rows between parallel fibers (Benjamin et al., 1995). The precise composition of the fibrocartilage is likely to depend on at least three factors: their developmental

TABLE 5. Resume of the tissue present through postmetamorphic development, shape, and dimensions of the osteological elements of the forelimb in anuran

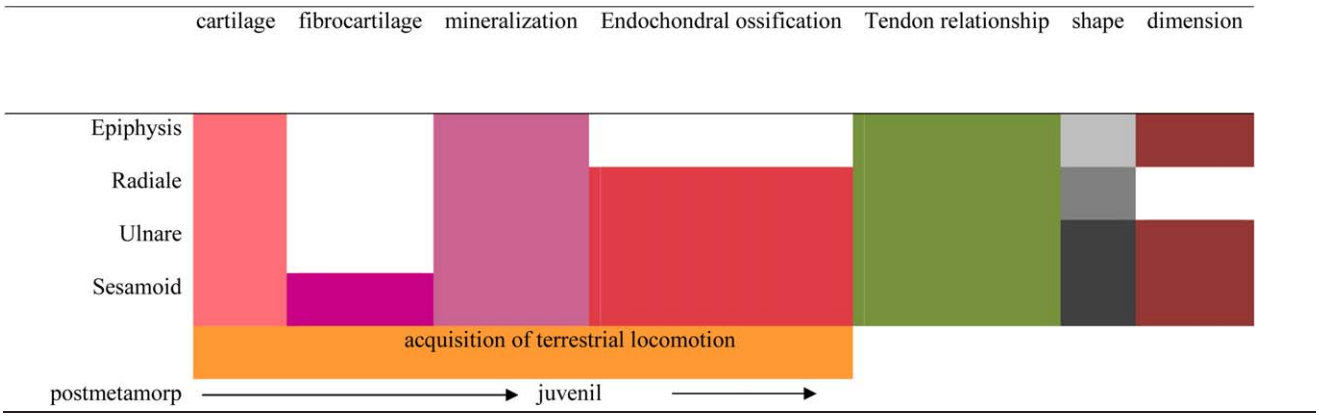

The same color in cells indicates common features among epiphyses of long bones, carpal bones and sesamoids in anurans. Orange cells indicate the change from aquatic to terrestrial locomotion parallel to tissue differentiation.

origins, the tensile loading, and age (Benjamin and Ralphs, 1998). Based on our data, we propose a tissue development sequence in the sesamoid: (1) cartilage (Ponssa et al., 2010; this work); (2) fibrocartilage; (3) mineralized ECM; and (4) endochondral bone (Table 5). This temporal sequence is reflected in the spatial gradation of the sesamoid tissues: the cartilage emerges from a fibrocartilaginous tissue connected to the tendon; this is to say that the fibrocartilage mediates between tissues of different physical constitution. The same general spatial configuration has been described in enthesis (Benjamin et al., 2006; Doherty, 2010), suggesting that this heterogeneity is related to the relation of tissues with different mechanical properties. In addition, it should be considered that both, fibrocartilage and mineralization are responses to a biomechanical challenge (Benjamin and Ralphs, 1998; Ralphs and Benjamin, 1994; Felisbino and Carvalho, 2001). Consequently, it seems reasonable that the ossification of sesamoids occur simultaneously with the acquisition of the full functionality of locomotion and with the passage to the terrestrial habitat, that is, in the juvenile phase of the anuran life, when they face a medium completely different in density, viscosity and gravitational force (Table 5) (Gillis and Blob, 2001). However, another explanation could complete this general picture. The constant presence of some sesamoids in particular groups (e.g., palmar sesamoid in most anurans and squamatas, Jerez et al., 2009; Ponssa et al., 2010) allow to infer an origin strongly linked to genetic stimulus (Ponssa et al., 2010). In addition, paralysis studies in frogs show sesamoids still form and mineralize with reduced or absent biomechanical input (Kim et al. 2009), which would not be expected if biomechanical loading is the only cause of sesamoid formation. Other paralysis studies suggest that the formation of the sesamoid anlage is genetically controlled, but extrinsic stimuli drive its differentiation (Abdala and Ponssa, 2012). It is likely both factors play important roles in the formation of all bones, varying mainly in relative proportion/timing.

Fabrezi et al. (2014) regarded the metamorphosis as a period implying that most important features for adult locomotion are already developed (e.g., girdles/limbs). However, the tissue differentiation of the structures implied in locomotion (e.g., osseus tissue) are still not mature, and it is later, through the juvenile development when is completed.

Long bone epiphyses, carpal bones, and sesamoids are all closely related to tendon. The early tendon is highly cellular and the longitudinal rows of cells become separated by ECM (Benjamin and Ralphs, 1997). The collagen fibers of the osteochondral ligament present between the periosteal bone and the lateral articular cartilage of the epiphyses are parallel to the axes of the long bone in the analyzed samples. On the contrary, in *Rana catesbeiana* the main fibers of collagen (types I and III) of the osteochondral ligament were found to be extended obliquely or perpendicular to the bone axis (Felisbino and Carvalho, 2000). The reasons for the modifications in fiber organization in the osteochondral ligament are not clear, but they may represent a mechanism to disperse load throughout the bone matrix (Felisbino and Carvalho, 2000).

Morphometric Analysis

The scatterplot of the PCA showed that both, ulnare and sesamoids are similar, whereas the radiale and the long bone epiphyses are highly different. In the morphometric analysis, only the radiale resulted with equivalent relative proportions of length and width, being the only element that would match the short bone definition, that is, length, width and height should be equivalent (Ross and Pawlina, 2007). According to our data, the category short bone, frequently used in many textbooks (Gravilov, 1959; Junqueira et al., 1992; Tortora and Derrickson, 2006; Ross and Pawlina, 2007) does apply neither to carpal bones nor to the sesamoids. We suggest that this ambiguous definition is useless to classify the normal endowment of skeletal bones and should be discarded. Thus, it was not possible to detect a common pattern of shape or morphometry between the carpal bones, and even less

between carpals and sesamoids or long bone epiphyses. Possibly the differences explained by the geometric morphometry analysis between ulnare and carpale are due to differences in the origin and ontogeny of these elements (Fabrezi, 1992; Fabrezi and Alberch, 1996; Fabrezi and Barg, 2001).

ACKNOWLEDGEMENT

All authors are grateful to CONICET, FONCyT and UNT for supporting our work via their research grants. They are grateful to Franco Pucci, Ana Pucci and Marisa Alcaide (Fundación Miguel Lillo) for their histological help.

APPENDIX 1
Eigen Values and Percentages for the Principal Components of the Contour Morphometric Geometric Analysis

	Eigenvalue	Proportion (%)	Cumulative (%)
PC1	1.517110E-002	43.2828	43.2828
PC2	7.018560E-003	20.0238	63.3067
PC3	3.151810E-003	8.9921	72.2987
PC4	2.983025E-003	8.5105	80.8092
PC5	1.604576E-003	4.5778	85.3870
PC6	1.521624E-003	4.3412	89.7282
PC7	7.983505E-004	2.2777	92.0059
PC8	5.424554E-004	1.5476	93.5535
PC9	4.302533E-004	1.2275	94.7810
PC10	3.724067E-004	1.0625	95.8435
PC11	2.563079E-004	0.7312	96.5747
PC12	1.836043E-004	0.5238	97.0985
PC13	1.453192E-004	0.4146	97.5131
PC14	1.165021E-004	0.3324	97.8455
PC15	1.061555E-004	0.3029	98.1484
PC16	8.538100E-005	0.2436	98.3919
PC17	8.305919E-005	0.2370	98.6289
PC18	6.547855E-005	0.1868	98.8157
PC19	5.380333E-005	0.1535	98.9692
PC20	5.054454E-005	0.1442	99.1134
PC21	4.285794E-005	0.1223	99.2357
PC22	3.596169E-005	0.1026	99.3383
PC23	3.367885E-005	0.0961	99.4344
PC24	2.693603E-005	0.0768	99.5112
PC25	2.218930E-005	0.0633	99.5745
PC26	1.911831E-005	0.0545	99.6291
PC27	1.616938E-005	0.0461	99.6752
PC28	1.496114E-005	0.0427	99.7179
PC29	1.415310E-005	0.0404	99.7583
PC30	1.052167E-005	0.0300	99.7883
PC31	9.887945E-006	0.0282	99.8165
PC32	8.430689E-006	0.0241	99.8405
PC33	8.237374E-006	0.0235	99.8641
PC34	6.863616E-006	0.0196	99.8836
PC35	6.049597E-006	0.0173	99.9009
PC36	5.488812E-006	0.0157	99.9166
PC37	4.933255E-006	0.0141	99.9306
PC38	4.198116E-006	0.0120	99.9426
PC39	3.520445E-006	0.0100	99.9526
PC40	2.708275E-006	0.0077	99.9604
PC41	2.531769E-006	0.0072	99.9676
PC42	2.058809E-006	0.0059	99.9735
PC43	1.952440E-006	0.0056	99.9790
PC44	1.727703E-006	0.0049	99.9840
PC45	1.482378E-006	0.0042	99.9882
PC46	1.131113E-006	0.0032	99.9914
PC47	1.061376E-006	0.0030	99.9945
PC48	9.215644E-007	0.0026	99.9971
PC49	5.474278E-007	0.0016	99.9986
PC50	4.750627E-007	0.0014	100.0000
PC51	1.120043E-018	0.0000	100.0000
PC52	4.506704E-020	0.0000	100.0000
PC53	2.629335E-020	0.0000	100.0000
PC54	2.294601E-020	0.0000	100.0000
PC55	1.542047E-020	0.0000	100.0000
PC56	7.952505E-021	0.0000	100.0000
PC57	6.216223E-021	0.0000	100.0000
PC58	5.051052E-021	0.0000	100.0000
PC59	3.352603E-021	0.0000	100.0000
PC60	2.895798E-021	0.0000	100.0000
PC61	1.717373E-021	0.0000	100.0000
PC62	1.056774E-021	0.0000	100.0000
PC63	5.775427E-022	0.0000	100.0000
PC64	2.121933E-022	0.0000	100.0000
PC65	−5.630339E-022	0.0000	100.0000
PC66	−7.998032E-022	0.0000	100.0000
PC67	−1.349949E-021	0.0000	100.0000
PC68	−1.662556E-021	0.0000	100.0000
PC69	−1.951877E-021	0.0000	100.0000
PC70	−2.383037E-021	0.0000	100.0000
PC71	−3.149249E-021	0.0000	100.0000
PC72	−3.673008E-021	0.0000	100.0000
PC73	−6.239967E-021	0.0000	100.0000
PC74	−1.099636E-020	0.0000	100.0000
PC75	−1.601198E-020	0.0000	100.0000
PC76	−2.201115E-020	0.0000	100.0000
PC77	−3.744892E-020	0.0000	100.0000
Total variance:	3.505107E-002		

LITERATURE CITED

Abdala V, Ponssa ML. 2012. Life in the slow lane: the effect of reduced mobility on tadpole limb development. Anat Rec 295:5–17.

Benjamin M, Ralphs JR, Shibu M, Irwin M. 1993. Capsular tissues of the proximal interphalangeal joint: normal composition and effects of dupuytren's disease and rheumatoid arthritis. J Hand Surg 18B:371–376.*[PMC]*[8345272*]*

Benjamin M, Qin S, Ralphs JR. 1995. Fibrocartilage associated with human tendons and their pulleys. J Anat 187:625–633.

Benjamin M, Ralphs JR. 1997. Tendons and ligaments—an overview. Histol Histopathol 12:1135–1144.

Benjamin M, Ralphs JR. 1998. Fibrocartilage in tendons and ligaments: an adaptation to compressive load. J Anat 193:481–494.

Benjamin M, Toumi H, Ralphs JR, Bydder G, Best TM, Milz S. 2006. Where tendons and ligaments meet bone : attachment sites ("entheses") in relation to exercise and/or mechanical load. J Anat 208:471–490.

Bierbaum RM, Ferson S. 1986. Do symbiotic pea crabs decrease growth rate in mussels? Biol Bull 170:51–61.

Bland YS, Ashhurst DE. 1997. Fetal and postnatal development of the patella, patellar tendon and suprapatella in the rabbit; changes in the distribution of the fibrillar collagens. J Anat 190: 327–342.

Bonucci E, Gomez S. 2012. Cartilage calcification. In: Jong Seto editor. Advanced topics in biomineralization. Rijeka: InTech. p 85–111.

Carter DR, Mikic B, Padian K. 1998. Epigenetic mechanical factors in the evolution of long bone epiphyses. Zool J Linn Soc 123:163–178.

Cei JM. 1980. Amphibians of argentina. Monitore Zoologico Italiano (N.S.) Monografia 2:1–609.
Dellorbo C, Gioglio L, Quacci D. 1992. Morphology of epiphyseal apparatus of a ranid frog (*Rana esculenta*). Histol Histopathol 7: 267–273.
Diaz G, Zuccarelli A, Pelligra I, Ghiani A. 1989. Elliptic Fourier analysis of cell and nuclear shapes. Comput Biomed Res 22:405–414.
Dickson RG. 1982. Ultrastructure of growth cartilage in the proximal femur of the frog, *Rana temporaria*. J Anat 135:549–564.
Di Rienzo JA, Casanoves F, Balzarini MG, Gonzalez L, Tablada M, Robledo CW. InfoStat versión. 2013. Grupo InfoStat, FCA, Universidad Nacional de Córdoba, Argentina. Available at: http://www.infostat.com.ar.
Doherty ARH. 2010. Murine metapodophalangeal sesamoid bones: morphology and potential means of mineralization underlying function. Anat Rec 293:775–785.
Duellman WE, Trueb L. 1994. Biology of amphibians. 2nd ed. Baltimore: Johns Hopkins University Press editors.
Ecker A. 1889. The anatomy of the frog. Amsterdam: A. Asher and Co.
Fabrezi M. 1992. El carpo de los anuros. Alytes 10:1–29.
Fabrezi M, Alberch P. 1996. The carpal elements of anurans. Herpetologica 52:188–204.
Fabrezi M, Barg M. 2001. Patterns of carpal development among anuran amphibians. J Morphol 249:210–220.
Fabrezi M, Abdala V, Oliver MIM. 2007. Developmental basis of limb homology in lizards. Anat Rec 290:900−912.
Fabrezi M, Manzano AS, Abdala V, Lobo F. 2014. Anuran locomotion: ontogeny and morphological variation of a distinctive set of muscles. Evol Biol 41:308–326.
Felisbino SL, Carvalho HF. 1999. The epiphyseal cartilage and growth of long bones in *Rana catesbeiana*. Tissue Cell 31: 301–307.
Felisbino SL, Carvalho HF. 2000. The osteochondral ligament: a fibrous attachment between bone and articular cartilage in *Rana catesbeiana*. Tissue Cell 32:527–536.
Felisbino SL, Carvalho HF. 2001. Growth cartilage calcification and formation of bone trabeculae are late and dissociated events in the endochondral ossification of *Rana catesbeiana*. Cell Tissue Res 306:319–323.
Felisbino SL, Carvalho HF. 2002. Ectopic mineralization of articular cartilage in the bullfrog *Rana catesbeiana* and its possible involvement in bone structure. Cell Tissue Res 301:357–365.
Ferson SF, Rohlf FJ, Koehn RK. 1985. Measuring shape variation of two-dimensional outlines. Syst Zool 34:59–68.
Freeman H, 1974. Computer processing of line-drawing images. ACM Comput Surv 6:57–97.
Gillis GB, Blob RW. 2001. How muscles accommodate movement in different physical environments: aquatic vs. terrestrial locomotion in vertebrates. Comp Biochem Phys A Mol Integr Physiol 131:61–75.
Giori NJ, Beaupré GS, Carter DR. 1993. Cellular shape and pressure may mediate mechanical control of tissue composition in tendons. J Orthop Res 11:581–591.
Gravilov K. 1959. Curso de anatomía y fisiología comparadas. Esqueleto I. Tucumán: Universidad Nacional de Tucumán. p 119.
Haines RW. 1940. Note on the independence of sesamoid and epiphysial centres of ossification. J Anat 75:101–105.
Haines RW. 1942. Note on the independence of sesamoid and epiphysial centres of ossification. J Anat 75:101–105.
Hinchliffe JR, Johnson DR. 1983. Growth of cartilage. In: Hall BK, editor: Cartilage. Vol. II: Development, differentiation and growth. New York: Academic Press. p 255–296.
Humason G. 1962. Animal tissue techniques. San Francisco: W. H. Freeman and Company.
Iwata H, Ukai Y. 2002. SHAPE: a computer program package for quantitative evaluation of biological shapes based on elliptic Fourier descriptors. J Hered 93:384–385.
Jerez A, Mangione S, Abdala V. 2009. Occurrence and distribution of sesamoid bones in squamates: a comparative approach. Acta Zool-Stockholm 91:295–305.
Junqueira LC, Carneiro J, Kelley RO. 1992. Basic histology. East Norwalk, United States: Appleton & Lange.
Kim HT, Olson WM, Hall BK. 2009. Effects of hind limb denervation on the development of appendicular ossicles in the dwarf African clawed frog, *Hymenochirus boettgeri* (Anura: Pipidae). Acta Zool 90:352–358.
Landis WJ, Hodgens KJ, Song MJ, Arena J, Kiyonaga S, Marko M, Owen C, McEwen BF. 1996. Mineralization of collagen may occur on fibril surfaces: evidence from conventional and high-voltage electron microscopy and three-dimensional imaging. J Struct Biol 117:24–35.
Landis WJ, Silver FH. 2002. The structure and function of normally mineralizing avian tendons. Comp Biochem Physiol A 133:1135–1157.
Laurie CC, True JR, Liu J, Mercer JM. 1997. An introgression analysis of quantitative trait loci that contribute to a morphological difference between *Drosophila simulans* and *D. mauritiana*. Genetics 145:339–348.
LeMinor JM. 1987. Comparative anatomy and significance of the sesamoid bone of the peroneus longus muscle (os peroneum). J Anat 151:85–99.
Lewis AR, Ralphs JR, Kneafsey B, Benjamin M. 1998. Distribution of collagens and glycosaminoglycans in the joint capsule of the proximal interphalangeal joint of the human finger. Anat Rec 250:281–291.
Liu J, Mercer JM, Stam LF, Gibson GC, Zeng ZB, Laurie CC. 1996. Genetic analysis of a morphological shape difference in the male genitalia of *Drosophila simulans* and *D. mauritania*. Genetics 142:1129–1145.
McDiarmid RW, Altig R. 1999.Tadpoles: the biology of anuran larvae. Chicago, USA: University of Chicago Press.
Olson W. 2000. Phylogeny, ontogeny, and function: extraskeletal bones in the tendons and joints of *Hymenochirus boettgeri* (Amphibia: Anura: Pipidae). Zoology 103:15–24.
Ponssa ML, Goldberg J, Abdala V. 2010. Sesamoids in anurans: new data, old issues. Anat Rec 293:1646−1668.
Prochel J. 2006. Early skeletal development in *Talpa europaea*, the common european mole. Zool Sci 23:427–434.
Ralphs JR, Benjamin M. 1994. The joint capsule: structure, composition, ageing and disease. J Anat 184:503−509.
Ralphs JR, Benjamin M. 1998. Fibrocartilage in tendons and ligaments—an adaptation to compressive load. J Anat 193:481–494.
Rohlf FJ. 1990. Fitting curves to outlines. In: Rohlf FJ, Bookstein FL, editors: Proceedings of the Michigan morphometrics workshop. Special Publication Number 2—The University of Michigan Museum of Zoology, Ann Arbor, Michigan. p 167–77.
Rohlf FJ, Archie JW. 1984. A comparison of Fourier methods for the description of wing shape in mosquitoes (rirera culicidae). Syst Zool 33:302–317.
Ross MH, Pawlina W. 2007.Tejido Óseo. – pp. 218–257 In: Lippincott Williams and Wilkins, Inc. (ed.): Histología, texto y atlas color con biología celular y molecular. – United States.
Rozenblut B, Ogielska M. 2005. Development and growth of long bones in european water frogs (Amphibia: Anura: Ranidae), with remarks on age determination. J Morphol 265:304−317.
Rufai A, Benjamin M, Ralphs JR. 1992. Development and aging of phenotypically distinct fibrocartilage associated with the rat achilles tendon. Anat Embryol 186:611–618.
Rufai A, Ralphs JR, Benjamin M. 1995. Structure and histopathology of the insertional region of the human achilles tendon. J Orthopaed Res 13:585–593.
Sarin VK, Erickson GM, Giori NJ. 1999. Coincident development of sesamoid bones and clues to their evolution. Anat Rec 257:174–180.
Sarin VK, Carter D. 2000. Mechanobiology and joint conformity regulate endochondral ossification of sesamoid. J Orthopaed Res 18: 706–712.
Shearman RM, Maglia AM. 2015. Osteological development of cope's gray treefrog, *Hyla chrysoscelis*. Acta Zool 96:181–198.
Sheets HD, Covino KM, Panasiewicz JM, Morris SR. 2006. Comparison of geometric morphometric outlines methods in the

discrimination of age-related differences in feather shape. Front Zool 3:15-

StatSoft, Inc. 2004. Statistica (data analysis software system), Version 7. Available at: www.statsoft.com.

ToroIbacache MV, Manriquez SG, Suazo GI. 2010. Geometric morphometrics and the study of biologic shapes: from descriptive to quantitative morphology. Int J Morphol 28:977–990.

Tortora GJ, Derrickson BH. 2006. Principios de Anatomía y Fisiología. Argentina: Médica-Panamericana, Buenos Aires.

Van'tVeen SJ, Hagen JW, Van Ginkel FC, Prahl-Andersen B, Burger EH. 1995. Intermittent compression stimulates cartilage mineralization. Bone 17:461–465.

Vera MC, Ponssa ML. 2014. Skeletogenesis in anurans: cranial and postcranial development in metamorphic and postmetamorphic stages of *Leptodactylus bufonius* (Anura: Leptodactylidae). Acta Zool 95:44–62. Stockholm

Vickaryous MK, Olson WM. 2007. Sesamoids and Ossicles in the Appendicular Skeleton. In: Hall BK, editor. Fins into limbs: evolution, development, and transformation. Chicago: University of Chicago Press. p 323–341.

Yoshioka Y, Iwata H, Ohsawa R, Ninomiya S. 2004. Analysis of petal shape variation of primula sieboldii by elliptic fourier descriptors and principal component analysis. Ann Bot 94: 657−664. London